

# Alpha-Particle Confinement Control of the Geodesic Winding of LHD-Type Fusion Reactors<sup>\*)</sup>

Tsuguhiro WATANABE

*National Institute for Fusion Science, Toki 509-5292, Japan*

(Received 15 November 2012 / Accepted 9 April 2013)

It is calculated that the geodesic winding D-shaped helical magnetic field configuration can actively control the confinement and exhaust of alpha particles. A trapped particle orbit diagram (TPOD), which shows the presence of re-entering particles and specifies the loss-cone depth, is obtained from the deeply trapped particle orbits in a helical mirror magnetic field. The loss-cone depth becomes shallow when the magnetic axis is shifted to the inner side. On the other hand, the loss-cone depth can reach to the magnetic axis when the magnetic axis is shifted fairly to the outer side. Active control of the confinement and exhaust of 3.52 MeV alpha particles by controlling the magnetic axis position is also confirmed by collisionless orbit calculations.

© 2013 The Japan Society of Plasma Science and Nuclear Fusion Research

Keywords: LHD, FFHR, geodesic winding, 3.52 MeV alpha particle, ash exhaust

DOI: 10.1585/pfr.8.2403072

## 1. Introduction

LHD-type magnetic configuration ( $\ell = 2$  Heliotron configuration) is produced by continuous helical and vertical coil systems. LHD experiments have achieved an average beta value of 5% without beta collapse. The high helical symmetry of the magnetic surface with an elliptical cross-section and good confinement of high-energy particles of standard LHD configurations has been numerically confirmed [1].

The LHD helical coils are wound as  $\chi = p\phi + \alpha_c \sin p\phi$  on a torus with a circular cross-section (the major radius is  $R_0 = 3.9$  m and the minor radius of the helical coil center is  $a_c = 0.975$  m) with a small pitch modulation factor  $\alpha_c = 0.1$ .  $p$  is the helical pitch number ( $\equiv m/\ell = 5$ ) and  $\chi$ ,  $\phi$  is the poloidal and toroidal angle, respectively.

In LHD-type fusion reactor (FFHR) design studies, the balance of blanket space ( $\equiv \delta$ : the narrowest space between the chaotic field lines and the inner wall of the helical coils) and the plasma volume are important. Kozaki pointed out that the dependence of the coil pitch parameter  $\gamma (= p a_c / R_0)$  of the magnetic structure is essential in LHD-type reactors. It is critically sensitive not only for optimizing the plasma volume but also for selecting the optimum blanket conditions [2]. Sufficient blanket space is necessary for adequate tritium breeding and shielding the magnet. For this purpose, the small  $\gamma$  configuration is preferable, but it leads to reduction in the plasma volume.

For the compatibility of the sufficient blanket space and the large plasma volume in reduced-size helical reactors, the D-shaped cross-section of the last closed flux surface (LCFS) was studied [3]. If the cross-section of

the magnetic surface becomes concave to the helical coils, it becomes easy to prepare the sufficient blanket space. For this purpose, the magnetic configuration is constructed by helical coils wound along the geodesic line of a torus, which we call the “winding frame” for the helical coils [3]. The effective value of the coil pitch parameter  $\gamma$  of the geodesic line is reduced (increased) in the inboard (outboard) side of the torus. Therefore, sufficient space between the first wall and the LCFS is reserved, and the position of the magnetic axis shifts close to the center of the two helical coils, which leads to a large plasma volume and the formation of a magnetic well. Helical coils wound along the geodesic line of a torus with an elongated cross-section can produce magnetic configurations with D-shaped magnetic surface, with magnetic well in the core region and high magnetic shear in the peripheral region. However, in general, the alpha-particle confinement of the geodesic winding helical reactor is poor compared to the LHD configuration. The performance of the DT alpha-particle confinement improves by increasing of the elongation factor  $\kappa$  of the cross-section of the winding frame. Nonetheless, the direct loss rate of alpha particles reaches 13% for an elongation factor  $\kappa = 1.8$  [3].

In order to search for higher performance magnetic field configurations, we have calculated the magnetic field by introducing a new winding frame of the helical coils. To improve the efficiency of the analysis of the performance of the magnetic field to alpha-particle confinement, we have developed a new diagram, the “trapped particle orbit diagram (TPOD).” The TPOD is useful for evaluating the performance of the high-energy particle confinement in a helical system without particle orbit calculations. The diagram shows that the loss-cone depth becomes shallow in

author's e-mail: watanabe.tsuguhiro@toki-fs.jp

<sup>\*)</sup> This article is based on the presentation at the 22nd International Toki Conference (ITC22).

the geodesic winding D-shaped helical magnetic field configuration when the magnetic axis is shifted to the inner side. On the other hand, the loss-cone depth can reach to the magnetic axis when the magnetic axis is shifted fairly to the outer side. Thus, the dynamic control of the alpha-particle confinement performance becomes feasible by controlling the position of the magnetic axis.

In Sec. 2, we describe the TPOD and apply it to the LHD-type magnetic configuration. In Sec. 3, we describe the helical winding coil along the geodesic line on the torus with a new elongated cross-section. It is shown that the geodesic winding D-shaped helical magnetic field configuration can actively control the confinement and the exhaust of alpha particles. We discuss the results in Sec. 4.

## 2. Trapped Particle Orbit Diagram

In a helical system, the particles are classified into three types: passing particles, chaotic orbit particles, and reflecting particles according to the ratio of the velocity component parallel to the magnetic field and the velocity component perpendicular to the magnetic field ( $v_{\parallel}/v_{\perp}$ ). The performance of a helical-type nuclear fusion reactor is strongly influenced by the orbit of the reflective particles whose characteristics can be analyzed by the orbit of deeply trapped particles. The orbit is uniquely determined by the condition of being trapped in the bottom of the helical magnetic mirror and of drifting on a constant magnetic field intensity surface

$$\left. \begin{aligned} 0 &= \frac{\mathbf{B}}{|\mathbf{B}|} \cdot \nabla |\mathbf{B}|, & 0 < \left( \frac{\mathbf{B}}{|\mathbf{B}|} \cdot \nabla \right)^2 |\mathbf{B}| \\ |\mathbf{B}| &= \text{const.} \end{aligned} \right\}. \quad (1)$$

Mod-Bmin contours projected on the poloidal cross section have been used to evaluate the global collisionless particle confinement [4]. However, the evaluation of particle confinement through Mod-Bmin contours projected on the poloidal cross-section becomes difficult when the magnetic field has two or more bottoms of a helical magnetic mirror. Furthermore, because the typical Mod-Bmin contour is constructed using a magnetic coordinates system, a realistic particle loss cannot be evaluated, on account of the trapped particles that are confined in the outside region of the LCFS in LHD-type magnetic configurations [1, 5].

Therefore, we have developed a ‘‘trapped particle orbit diagram (TPOD)’’ using a real coordinates system that can describe the shape of the vacuum vessel wall. Drift orbits given by eq. (1) are solved numerically. Starting points are allocated on multiple poloidal planes to correspond to the case of multiple bottoms of the helical magnetic mirror. The particle-loss boundary is set at the vacuum vessel wall.

Particles become loss-cone particles (direct-loss particles) if the trajectory given by eq. (1) reaches the vacuum vessel wall. When the trajectory gets across the LCFS but does not reach the vacuum vessel wall, the particle is a confined particle (re-entering particle). When the local mini-

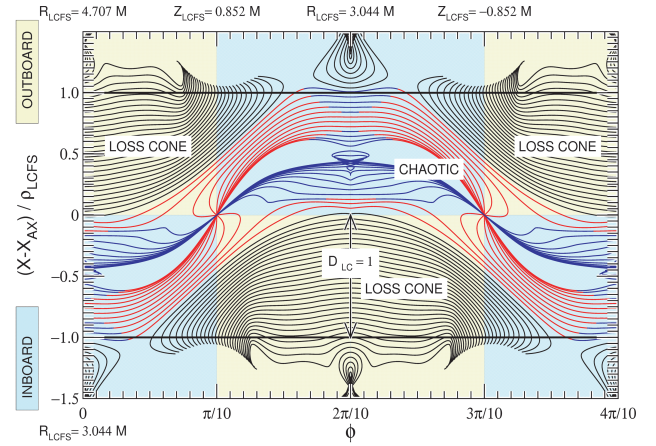


Fig. 1 TPOD for the magnetic field produced by the helical coils whose winding law is given by eq. (3). The horizontal axis is the toroidal angle  $\phi$  ( $\phi = 0, 2\pi/10, 4\pi/10$ , is for the horizontally long cross-section, and  $\phi = \pi/10, 3\pi/10$  is for the vertically long cross-section of the magnetic surfaces). The vertical axis  $X$  is the rotating helical coordinate along the long axis of the magnetic surface.  $X_{ax}$  is the position of the magnetic axis and  $\rho_{lcfs}$  is the minor radius of the LCFS. The loss-cone orbits are shown by the black dots. The trapped particle orbits in the local minimum of the helical mirror are shown by the red dots. The blue dots represent the orbits passing through the local maximum points satisfying the condition given by eq. (2). The loss-cone depth is the distance of the deepest surface of the loss-cone particles measured from the LCFS.  $D_{LC}$  is the normalized value of the loss-cone depth by the minor radius of the LCFS ( $= \rho_{lcfs}$ ).  $D_{LC} = 1$  shows that loss-cone particles exist even on the magnetic axis.  $D_{LC} = 0$  shows that loss-cone particles do not exist inside the LCFS.

mum  $|\mathbf{B}|$  condition breaks

$$0 > \left( \frac{\mathbf{B}}{|\mathbf{B}|} \cdot \nabla \right)^2 |\mathbf{B}|, \quad (2)$$

the deeply trapped particle orbit becomes chaotic. When the local minimum  $|\mathbf{B}|$  condition breaks outside of LCFS, the particle becomes a chaotic orbit particle with a finite life time and flows out to a divertor tile along the divertor leg.

First, in Fig. 1, we show the TPOD of the magnetic configuration in which the performance of high-energy particle confinement is poor although the form of the magnetic surface is excellent. The magnetic field is produced by LHD-type helical coils with relatively large pitch modulation factor  $\alpha_c$  compared to the LHD

$$\chi = p\phi + \alpha_c \sin p\phi, \quad \alpha_c = 0.4. \quad (3)$$

The TPOD in Fig. 1 indicates that the large majority of deeply trapped particles cannot be confined and flow into the vacuum vessel wall regardless of the divertor legs. We confirmed this by the particle orbit computations using the magnetic field produced by the helical coils with

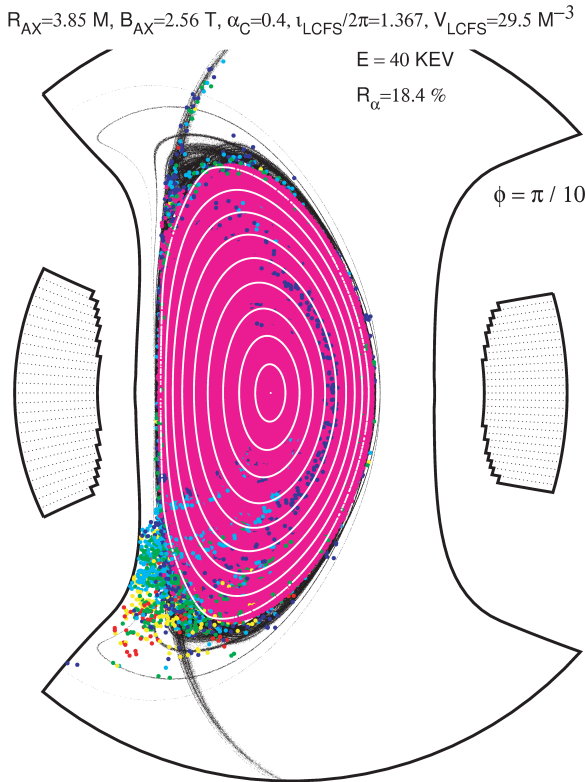


Fig. 2 Poincaré plots of  $E = 40 \text{ keV}$  protons corresponding to the TPOD given by Fig. 1. The chaotic field lines are shown by the very small black dots and the closed magnetic surfaces are shown by the tiny white dots. The direct loss rate of  $E = 40 \text{ keV}$  protons is  $R_\alpha = 18.4\%$ .

eq. (3). Birth points are equally distributed inside the magnetic surface ( $\rho/\rho_{LCFS} \leq 0.8$ ) with uniformly distributed initial pitch angles. The upper limit of the numerical computation is set to 1.2519 ms, which is the time needed to reach 100 toroidal turns ( $= 10^3$  helical pitch) of thermal speed of  $E = 40 \text{ keV}$  protons. This time is sufficient to distinguish between integrable orbits and chaotic orbits. Moreover, because the chaotic orbit particles with a life time longer than the upper limit computation time are few, the particles that remain in the vacuum vessel after the end of the computation are treated as confined particles. Poincaré plots of  $E = 40 \text{ keV}$  protons, whose orbits are equivalent to the 3.52 MeV alpha particles in a DT fusion reactor with  $R_0 = 13 \text{ m}$  and  $B_0 = 7 \text{ T}$  are shown in Fig. 2. Puncture points are color-coded according to the life time  $\tau$  of the  $E = 40 \text{ keV}$  protons:

- red:  $0.0000 < \tau(\text{ms}) \leq 0.0125$
- yellow:  $0.0125 < \tau(\text{ms}) \leq 0.0250$
- green:  $0.0250 < \tau(\text{ms}) \leq 0.0626$
- cyan:  $0.0626 < \tau(\text{ms}) \leq 0.1252$
- blue:  $0.1252 < \tau(\text{ms}) \leq 0.1252$
- magenta:  $1.2519 < \tau(\text{ms})$

The LHD helical coils have a small pitch modulation

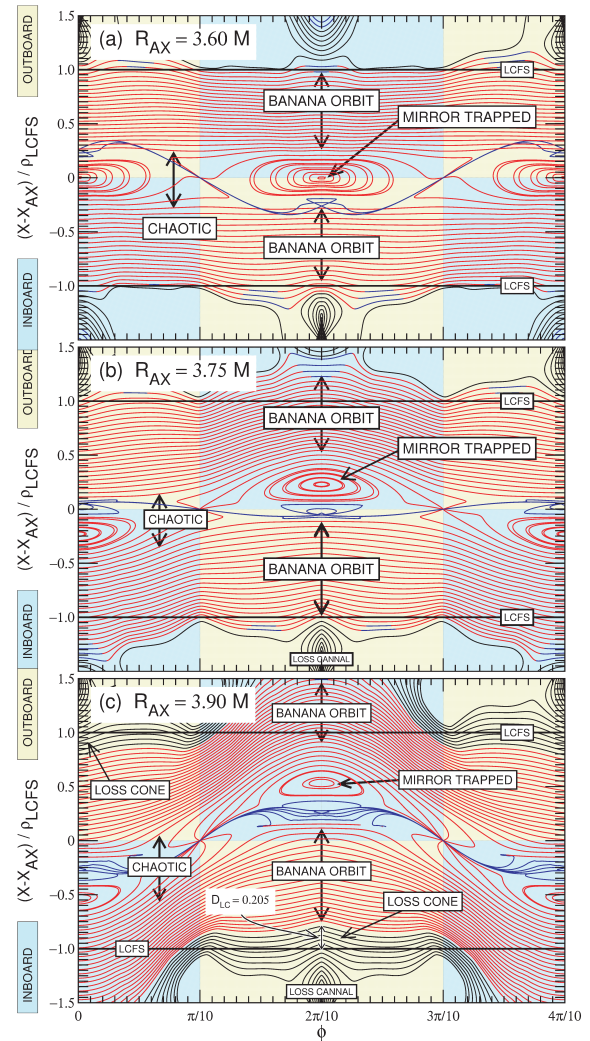


Fig. 3 The TPOD for the typical magnetic configuration of the LHD. (a): For the case of the standard configuration  $R_{ax} = 3.6 \text{ m}$  (inner magnetic axis case). Loss-cone orbit is not present. There are few re-entering particles. (b): For the case of another standard configuration  $R_{ax} = 3.75 \text{ m}$  (outer magnetic axis case). Loss-cone orbit is not present. There are re-entering particles not few. (c): For the case of one of large outer magnetic axis position,  $R_{ax} = 3.9 \text{ m}$ . A shallow loss-cone region exists. There are many re-entering particles.

of  $\alpha_c = 0.1$ . This small pitch modulation was determined by considering the gap distance between the first wall and LCFS, and the confinement properties of the high-energy particles [6]. The TPOD for the typical magnetic configuration of the LHD is shown in Fig. 3. This diagram shows that banana orbits in the inner shift magnetic axis configuration are bound almost on one magnetic surface, as shown in Fig. 3 (a). On the other hand, banana orbits in the outer shift magnetic configuration traverse the magnetic surface and produce re-entering particles, as shown in Figs. 3 (b,c). The loss-cone region does not exist in the standard configurations as shown in Figs. 3 (a,b) ( $D_{LC} = 0$ ). A shallow loss-cone region exists for the large outer shifted magnetic axis

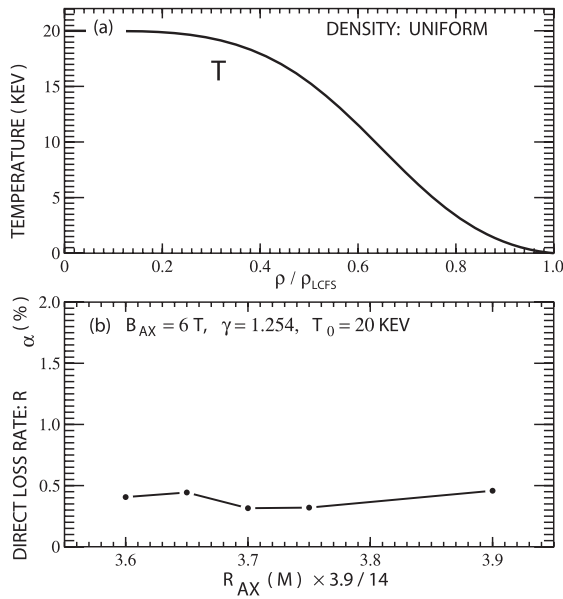


Fig. 4 (a): Temperature profile as a function of the minor radius  $\rho$  of the magnetic surface. (b): Collisionless loss rate of 3.5 MeV particles in the LHD magnetic field configuration. The horizontal axis shows the major radius of the magnetic axis.

configuration, as shown in Fig. 3 (c). We have confirmed through particle orbit calculations that no re-entering particles protrude from the boundary of the chaotic field lines. In regions near the magnetic axis of the horizontally long cross-section of the magnetic surface, there are helical mirror-trapped particles that do not circulate around the torus. On the other hand, near the magnetic axis of vertically long cross-section of the magnetic surface, all deeply trapped reflecting particles become chaotic orbit particles that circulate around the torus.

To see the influence of the loss-cone depth, we have calculated the direct loss rate of alpha particles for a fusion reactor with a similar extension of the LHD. The probability of the birth position of 3.52 MeV alpha particles is calculated under the condition of uniform density distribution and temperature distribution shown in Fig. 4 (a).

The loss-cone depth  $D_{LC}$  is reflected in the direct loss rate of 3.52 MeV alpha particles; however, the effect is small. The performance of the LHD magnetic field configuration is very high for the confinement of 3.52 MeV, as shown in Fig. 4 (b).

### 3. Geodesic Winding Helical Coils and Alpha-Particle Confinement Control by Magnetic Axis Position Control

The geodesic winding on a toroidal surface with a constant major radius  $R$  and a constant minor radius  $a$  was studied for the superconducting magnetic energy storage (SMES) [7] to reduce the electromagnetic stress working

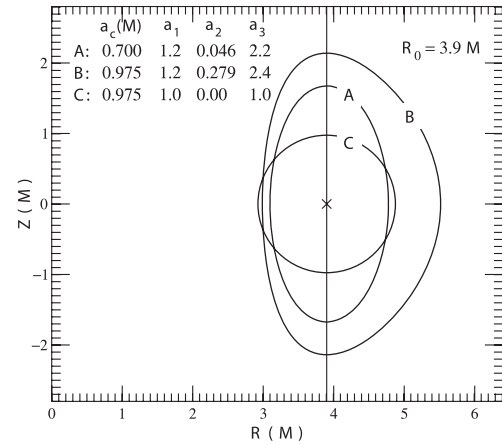


Fig. 5 “A” is the winding frame of the helical coils used in the present paper. “C” is the winding frame of the LHD helical coils.

in coils systems. In order to express the various types of winding frames with only a few parameters ( $a_1, a_2, a_3$ ), we use the following form for the cross-section of the winding frame

$\chi$  : poloidal angle

$R_0$  : major radius of the helical coil

$a_c$  : minor radius of the helical coil

$$r - R_0 = a_c \times \frac{a_1}{1 - a_2 \cos \chi} \cos \chi, \quad (4)$$

$$z = a_c \times a_3 \sin \chi, \quad (5)$$

where  $r$  and  $z$  are the standard cylindrical coordinates. Figure 5 shows the examples of the D-shaped winding frame, including the winding frame of the LHD. The construction of the geodesic winding helical coils is carried out by the same procedure as that in [3]. An example of the helical coils and the assembly of helical coils, the vertical magnetic field coils, and the vacuum vessel is shown in Fig. 6.

The volume of magnetic surface  $V_{lcf}$ , the thickness of the chaotic field line layer, and the compactness of the divertor field lines significantly change depending on the vertical magnetic field coils. Figure 7 shows a Poincaré plot of lines of force under a carefully selected configuration of vertical magnetic field coils. The winding frame of the helical coils is described as “A” in Fig. 5.

The compatibility of the sufficient blanket space and the large plasma volume is satisfied in a reduced-size helical reactor ( $V_{lcf} = 71.6 \text{ m}^3$ ,  $R_{ax} = 3.9 \text{ m}$ ).

The distributions of the specific volume  $U$  and the rotational transform  $\iota/2\pi$  are shown in Fig. 8. A magnetic well exists ( $\delta U/U_{ax} = 0.021$ ) in the core plasma region, and high magnetic shear is present in the peripheral region.

The TPOD for the geodesic winding D-shaped helical magnetic field configurations are shown in Fig. 9, for the case of inner and outer magnetic axis configurations.

This diagram shows that no re-entering particles exist in these geodesic winding D-shaped helical magnetic

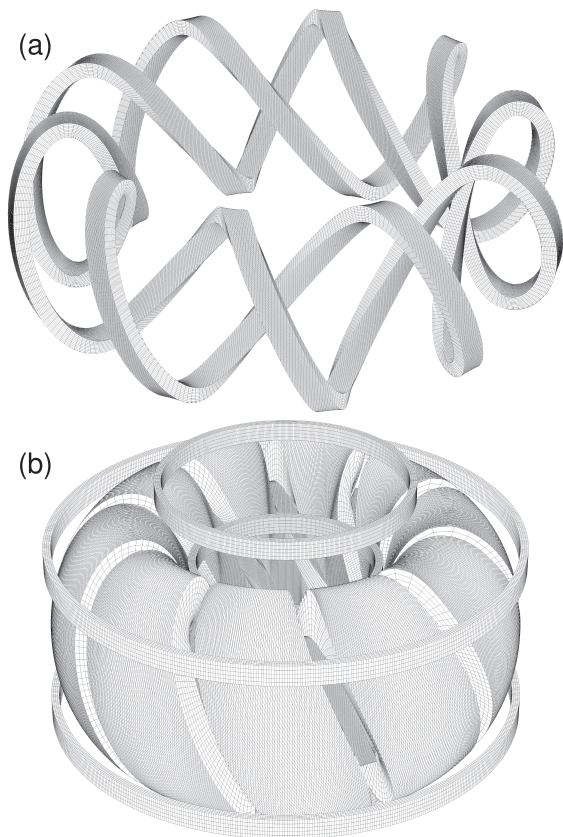


Fig. 6 (a): Geodesic winding helical coils with winding frame “A” shown in Fig. 5. (b): Assembly of helical coils, vertical magnetic field coils, and vacuum vessel.

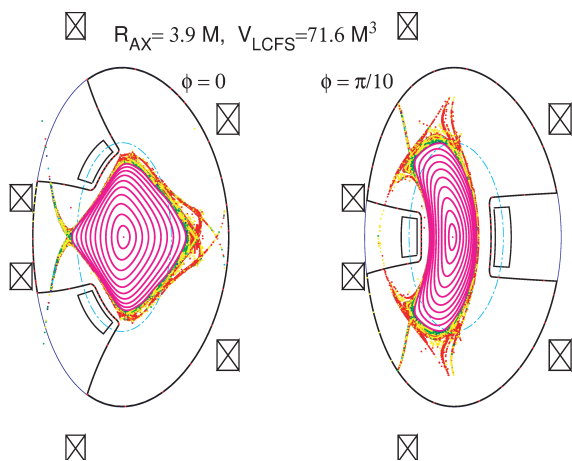


Fig. 7 Poincaré plot of lines of force at the poloidal cross-section at  $\phi = 0$  and  $\phi = \pi/10$ . The cross-sections of the helical coils, vertical field coils, and the vacuum vessel are also shown. The cross-section of the winding frame for the helical coils is also shown by cyan chain line.

field configurations. The loss-cone depth  $D_{LC}$  becomes shallow for the inner shift magnetic axis configuration. For the large outer shift magnetic axis configuration, the loss-cone depth reaches the magnetic axis as shown in Fig. 9 (b). Thus, the geodesic winding D-shaped helical magnetic field configuration can actively control the con-

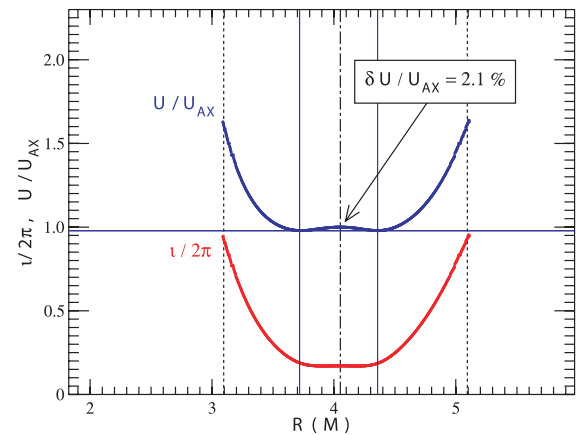


Fig. 8 Distribution of the rotational transform (red) and the specific volume (blue) of lines of force (case for  $R_{ax} = 4 \text{ m}$ ). The horizontal axis  $R$  is the major radius at the  $\phi = 0$  poloidal cross-section. The position of the magnetic axis and the positions of the LCFS are shown by chain line and broken lines, respectively.

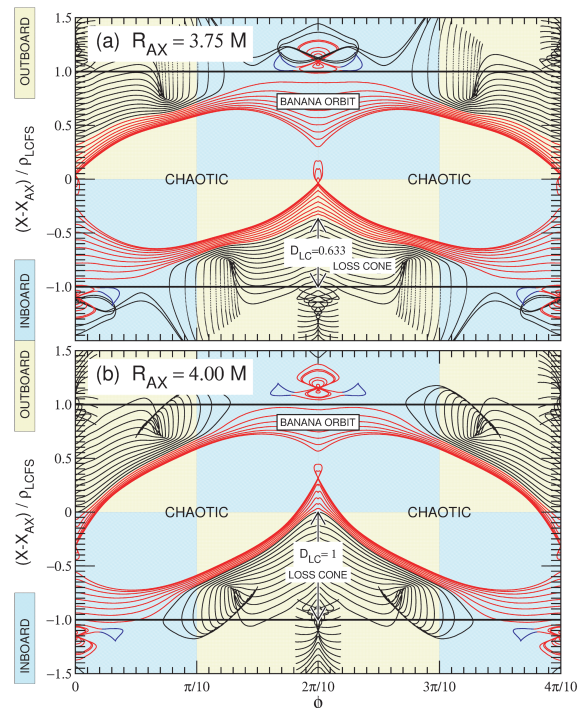


Fig. 9 The TPOD for the geodesic winding D-shaped helical magnetic field configuration. (a): For the case of the inner magnetic axis case ( $R_{ax} = 3.75 \text{ m}$ ). (b): For the case of the large outer magnetic axis position case ( $R_{ax} = 4.0 \text{ m}$ ).

finement and exhaust of alpha particles by controlling the shift of the magnetic axis position.

To confirm this possibility, we have performed the numerical computations of the collisionless orbit of 3.52 MeV alpha particles. The birth position of alpha particles is uniform inside the magnetic surface of  $\rho/\rho_{LCFS} \leq 0.8$ . The initial pitch angle is also uniform in the range  $[0, \pi]$ .

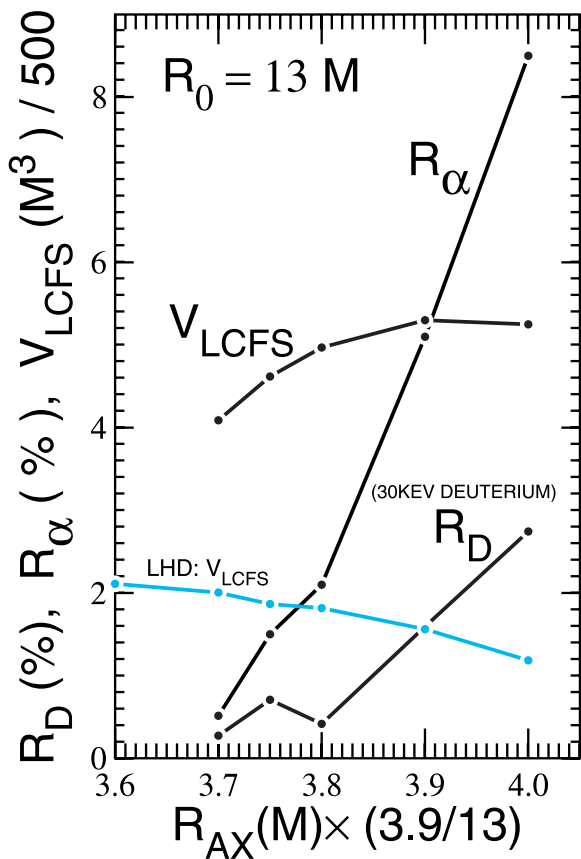


Fig. 10 The dependence of the magnetic axis position  $R_{ax}$  to the direct loss rate of 3.52 MeV alpha particle ( $R_{\alpha}$ ) and of fuel ions ( $R_D$  for 30 keV deuterium), in the geodesic winding D-shaped helical magnetic field configuration. The magnetic axis positional dependence of the volume of the LCFS  $V_{LCFS}$ , in the case of a geodesic winding fusion reactor and of the LHD winding fusion reactor are also shown. The major radius of helical coils is assumed to be  $R_0 = 13$  m.  $B_{ax} = 7$  T.

The numerical results are summarized in Fig. 10. When the alpha particles are accumulated in the fusion reactor, the alpha-particle loss flux from the core plasma can be increased by the outer shift of the magnetic axis position, whereas the increase in the loss flux of the fuel plasma is suppressed low ( $R_D$  in Fig. 10).

#### 4. Discussion

To realize fusion reactors at an early stage, it is necessary to mitigate the severe engineering issues, by innovative concept of core plasma physics. We have proposed a geodesic winding helical reactor with D-shaped magnetic surface, based on the progress of LHD experimental re-

sults, design study of FFHR and experiences of tokamak.

The geodesic winding D-shaped helical magnetic field configuration has the following merits.

- The geodesic winding allows the tightening winding of the helical coils. Consequently, the helical coil winding is expected to be mechanically stable and easy to manufacture.
- The stability of the magnetic surface position, including the divertor leg structure.
- The stability of high-beta and high-density plasma because of the magnetic well in the core plasma region and the high magnetic shear in the peripheral region.
- The improvement in confinement because of the large plasma volume and D-shaped magnetic surface.
- Large horizontal ports can be set up in the geodesic winding D-shaped helical magnetic field configuration as shown in Fig. 6 (b).

In addition to the above-mentioned, we showed that the confinement and exhaust of alpha particles can be controlled in the geodesic winding D-shaped helical magnetic field configuration. Furthermore, the reduction of the coil magnetic stress by geodesic winding will be investigated in the future.

In a fusion reactor, it is expected that the plasma beta value exceeds 5% and the plasma current considerably modifies the vacuum magnetic field. However, because the LHD-type magnetic field configuration has three sets of vertical magnetic field coils, it can be expected that an optimal magnetic field similar to the vacuum case can be constructed by using appropriate current values of the vertical magnetic field coils. The confirmation of this possibility in finite beta plasma is a future research topic.

The author thanks the members of the Meeting on Helical Reactor Design at the National Institute for Fusion Science for discussions regarding helical reactor systems. The author also expresses his gratitude to Profs. Hiroaki Tsutsui and Shunji Iio for the geodesic winding of helical coils. This work was performed with the support and under the auspices of the NIFS Collaborative Research Programs NIFS10KNXN194 and NIFS11KNST026.

- [1] T. Watanabe *et al.*, Nucl. Fusion **46**, 291 (2006).
- [2] Y. Kozaki *et al.*, Nucl. Fusion **49**, 115011 (2009).
- [3] T. Watanabe, Plasma Fusion Res. **7**, 2403113 (2012).
- [4] M. Yokoyama *et al.*, Nucl. Fusion **40**, 261 (2000).
- [5] Y. Matsumoto *et al.*, J. Phys. Soc. Jpn. **71**, 1684 (2002).
- [6] N. Ohyabu *et al.*, Nucl. Fusion **34**, 387 (1994).
- [7] H. Tsutsui, T. Habuchi, S. Tsuji-Iio and R. Shimada, IEEE Trans. Appl. Supercond. **22**, 4705604 (2012).